Research article

On a data-driven mathematical model for prostate cancer bone metastasis

Zholaman Bektemessov[1,2,*]**, Laurence Cherfils**[2,*]**, Cyrille Allery**[2]**, Julien Berger**[2]**, Elisa Serafini**[2,3]**, Eleonora Dondossola**[4] **and Stefano Casarin**[2,3,5]

[1] Department of Mathematical and Computer Modeling, Al-Farabi Kazakh National University, Al-Farabi Ave. 71, Almaty, 050060, Kazakhstan

[2] Laboratoire des Sciences de l'Ingénieur pour l'Environnement, UMR CNRS 7356, La Rochelle Université, La Rochelle Cedex 1, F-17042, France

[3] Center for Precision Surgery, Houston Methodist Research Institute, Houston, TX, United States

[4] David H. Koch Center for Applied Research of Genitourinary Cancers, University of Texas MD Anderson Cancer Center, Houston, TX, United States

[5] Department of Surgery, Houston Methodist Hospital, Houston, TX, United States

* **Correspondence:** Email: zholaman.bektemessov@kaznu.edu.kz, laurence.cherfils@univ-lr.fr.

Abstract: Prostate cancer bone metastasis poses significant health challenges, affecting countless individuals. While treatment with the radioactive isotope radium-223 (^{223}Ra) has shown promising results, there remains room for therapy optimization. *In vivo* studies are crucial for optimizing radium therapy; however, they face several roadblocks that limit their effectiveness. By integrating *in vivo* studies with *in silico* models, these obstacles can be potentially overcome. Existing computational models of tumor response to ^{223}Ra are often computationally intensive. Accordingly, we here present a versatile and computationally efficient alternative solution. We developed a PDE mathematical model to simulate the effects of ^{223}Ra on prostate cancer bone metastasis, analyzing mitosis and apoptosis rates based on experimental data from both control and treated groups. To build a robust and validated model, our research explored three therapeutic scenarios: no treatment, constant ^{223}Ra exposure, and decay-accounting therapy, with tumor growth simulations for each case. Our findings align well with experimental evidence, demonstrating that our model effectively captures the therapeutic potential of ^{223}Ra, yielding promising results that support our model as a powerful infrastructure to optimize bone metastasis treatment.

1. Introduction

Prostate cancer (PCa) is the fifth leading cause of death from cancer worldwide and the most common malignancy in elderly men [5]. Bone metastasis, the most frequent complication in PCa, reduce life expectancy in patients with advanced PCa because they are unresponsive to conventional molecular targeting therapy [3]. Radium-223 (^{223}Ra), a bone-targeted radionuclide, has recently been approved for the treatment of bone metastasis, since it improves symptom-free and overall survival in patients with advanced metastatic PCa [26]. Despite encouraging evidence during early follow-up, clinical response is often followed by relapses and disease progression, and associated mechanisms of efficacy and resistance are poorly understood [26]. Research efforts to overcome this gap have been largely based on the use of animal models, which are useful but require a large investment of time and resources [22]. Computational models, integrated with animal data, can mitigate experimental limitations and better guide research at a preclinical level [32].

Several mathematical models have been developed to study the progression of many cancer types, from agent-based models (ABMs) [10], to partial differential equation (PDE) models [27, 30], and more specifically PCa [11]. However, to our knowledge, only a few papers address bone metastasis and the therapeutic effect of ^{223}Ra therapy. In [10, 13, 25], an ABM of PCa bone metastasis is developed where tumor cell mitosis and apoptosis are described as probability densities, and each cell (agent) is regulated by stochastic dynamics linked to the mentioned probability. While simulating ^{223}Ra administration, the bone becomes a reservoir for this drug and then the probability of mitosis and apoptosis of cancer cells depends on two factors: the distance from the cell to mineral bone, since ^{223}Ra reduces its effect toward the bone marrow in a distance-dependent fashion; and time, since the drug has an approximate 11-day half-life, meaning that the effect of ^{223}Ra on mitosis and apoptosis is halved after 11 days of follow-up.

While existing computational models detail spatial resolution through computationally intensive agent-based approaches, we propose a PDE model that retains spatial detail with a more efficient computational infrastructure. We hypothesize that this alternative approach will reduce computational costs and enhance accessibility, allowing faster iterations and easier integration into clinical workflows.

Accordingly, in this work, we develop a data-driven PDE model to simulate the effect of ^{223}Ra therapy on the PCa bone metastasis progression. We calibrated the model driving coefficients on metastatic cell line growth data provided by the David H. Koch Center for Applied Research of Genitourinary Cancers at MD Anderson Cancer Center, in Houston, Texas, USA.

Overall, we propose a computational resource-efficient infrastructure for the study of ^{223}Ra therapy that will facilitate broad usage, quick scenario testing, and real-time decision support, ultimately leading to more predictions of therapy outcomes.

2. The tumor growth mathematical model

2.1. The PDE model

Cancer cells are characterized by abnormally high mitosis and, as the other cells, they are subjected to standard diffusion laws. Their evolution can be described by the classical equation (see [19] for instance):

$$\begin{cases} \dfrac{\partial \hat{C}}{\partial t} - \rho \Delta \hat{C} = \alpha(t)\,\hat{C}(1 - \dfrac{\hat{C}}{\hat{C}_{max}}) - g(t)\hat{C} & \text{in } \Omega \times [0, T], \\[2mm] \nabla \hat{C} \cdot \mathbf{n} = 0 & \text{on } \partial\Omega \times [0, T], \\[2mm] \hat{C}(x, 0) = \hat{C}_0 & \text{in } \Omega, \end{cases} \quad (2.1)$$

in which $\hat{C} = \hat{C}(x, t)$ defines the tumor cell density at location x (cm) and time t (day), $\rho > 0$ ($cm^2 day^{-1}$) is the diffusion coefficient representing the motility of the tumor cells, $\alpha > 0$ (day^{-1}) represents the proliferation (mitosis) rate, and $g > 0$ (day^{-1}) is the apoptosis rate. We assume that $\alpha > g$. Moreover $\hat{C}_{max}$ is the carrying capacity (limiting the density of cells that a volume of tissue can hold), $\hat{C}_0$ is the initial distribution of the tumor cells, Ω is a bounded and regular domain of $\mathbb{R}^2$ standing for a part of the bone surrounding the tumor, and $\mathbf{n}$ is the unit normal to the domain boundary $\partial\Omega$.

When α and g are Lipschitz continuous and bounded functions, the well-posedness of this equation is well-known. The main results are summarized in the following theorem, whose proof can be found, for instance, in [28].

Theorem 2.1. *We assume that $\hat{C}_0$ belongs to $L^2(\Omega)$ and that $0 \leq \hat{C}_0(x) \leq \hat{C}_{max}$, $\forall x \in \Omega$. Then, problem (2.1) possesses a unique weak solution $\hat{C}$ in $L^\infty(0, T; L^2(\Omega)) \cap L^2(0, T; H^1(\Omega))$ which satisfies*

$$0 \leq \hat{C}(x, t) \leq \hat{C}_{max}, \quad \forall (x, t) \in \Omega \times [0, T].$$

In modeling the control condition (where the tumor growth is not subjected to therapy), we will consider the Eq (2.1) with constant α^0 (mitosis) and g^0 (apoptosis) rates. We note

$$\rho = \rho^0, \quad \alpha(t) = \alpha^0, \quad g(t) = g^0, \quad \forall t \in [0, T]. \quad (2.2)$$

Alternatively, in modeling tumor response to ^{223}Ra therapy, cancer cells are less diffusive, with impaired mitosis and with enhanced apoptosis, than control cancer cells. Then, as a first choice, we will consider Eqs (2.1) with the mitosis, apoptosis, and diffusion rates such that:

$$\rho = \rho^{rad}, \quad \alpha(t) = \alpha^{rad}, \quad g(t) = g^{rad}, \quad \forall t \in [0, T], \quad (2.3)$$

satisfying $\alpha^{rad} < \alpha^0$, $g^{rad} > g^0$, and $\rho^{rad} \leq \rho^0$, with α^0, g^0, and ρ^0 introduced in (2.2) for the control case (without ^{223}Ra therapy).

To take into account the decay of the ^{223}Ra treatment efficacy over time (11-day half-life), we will consider the alternative, more accurate model,

$$\rho = \rho^{rad}, \quad \alpha(t) = \frac{\alpha^0}{1 + re^{-t/\tau}}, \quad g(t) = \frac{g^0}{1 - re^{-t/\tau}}, \quad \forall t \in [0, T], \quad (2.4)$$

with α^0 and g^0 introduced in (2.2), and r and τ as positive constants. The parameter r is related to the treatment aggressiveness, while τ modulates the time-dependent effect of ^{223}Ra (see [10]).

2.2. The ODE model

The PDE model (2.1) involves several positive parameters (namely ρ, α, and g)[1] that can be determined using experimental observations of tumor cell growth obtained from animal experiments.

---

[1] (ρ^0, α^0, g^0) in (2.1)-(2.2), $(\rho^{rad}, \alpha^{rad}, g^{rad})$ in (2.1)-(2.3), (ρ^{rad}, r, τ) in (2.1)-(2.4)

However, due to experiment design constraints, only measured data of the evolution of the total number of cancer cells with respect to time are available. Therefore, the diffusion coefficient ρ cannot be retrieved. The model will be calibrated only regarding the mitosis α and apoptosis g rates.

Accordingly, we assume that the dependence on x of $\hat{C}$ is negligible, thus making $\hat{C}$ only depending on t, i.e. $\hat{C} = \hat{C}(t)$. We denote by C the total number of cancer cells in the tumor, and we have

$$C(t) = \hat{C}(t)|\omega|,$$

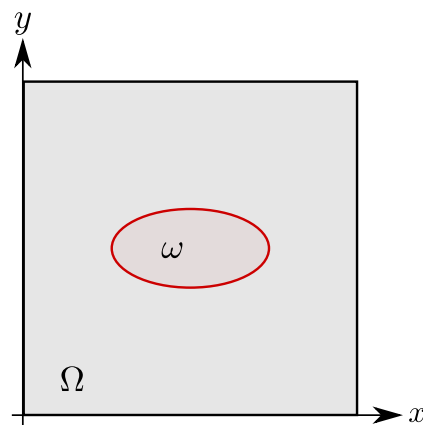with $\omega \subset \Omega$ being the (fixed in time) domain of the tumor, and $|\omega|$ its area.

Figure 1. Illustration of the tumor domain ω within the whole domain Ω.

Replacing $\hat{C} = \dfrac{C}{|\omega|}$ in (2.1), we obtain that C satisfies the equation

$$\begin{cases} \dfrac{\partial C}{\partial t} = \alpha(t)\,C(1 - \dfrac{C}{C_{max}}) - g(t)C, & t \in [0, T], \\ C(0) = C_0, \end{cases} \tag{2.5}$$

where $C_0 = \hat{C}_0\,|\omega|$ stands for the initial number of cancer cells in the tumor and $C_{max} = \hat{C}_{max}\,|\omega|$ is the maximum number of cancer cells. We emphasize that the same coefficients α and g appear in (2.1) and (2.5); however, it is worth noting that the value of C_{max} will differ for problems with and without treatment, as follows: C^0_{max} (without treatment) and C^{rad}_{max} (with treatment).

The rest of the paper is organized as follows. The coefficients α and g will be estimated using experimental data and considering the ordinary differential equation (ODE) model (2.5) in sections 3 and 4 for the two different cases: control (without ^{223}Ra therapy) and with ^{223}Ra therapy. With the retrieved parameters of mitosis and apoptosis, 2-D simulations of the tumor growth from the (2.1) model will be proposed in section 5.

3. Identifiability of the parameters in the ODE

This section describes the stages of solving the parameter estimation problem based on uniquely identifying a set of parameters $\boldsymbol{p} = (\alpha, C_{max}, g)$ of a mathematical model (2.5) in the form of differential equations, tools of identifiability analysis, and optimization algorithms for the objective function.

When working with unknown parameters, in most cases, the question arises whether it is possible to identify the unique set of parameters that fits the experimental data. The identifiability analysis helps in verifying that parameters can be estimated with satisfying accuracy.

3.1. Structural identifiability analysis

It is crucial first to verify whether the relevant parameters can be determined independently from the available data or measurements. Without this initial verification, the validity and reliability of the overall study may be compromised. If, based on the input data and measurement data, the set of parameters is unique, then the dynamic system can be called *structurally globally identifiable*, otherwise it is *unidentifiable* [18].

To prove the identifiability in our model, the definition is recalled based on [31]:

Definition 3.1. *Let* $C : \Omega_p \times [0, T] \rightarrow \mathbb{R}$, *an observable function associated with the parameter* $\boldsymbol{p} \in \Omega_p$. *The parameter* $\boldsymbol{p}$ *is structurally globally identifiable if we have the following condition:*

$$\forall \bar{\boldsymbol{p}} \in \Omega_p, \ \forall t \in [0, T], \quad C(\boldsymbol{p}, t) = C(\bar{\boldsymbol{p}}, t) \Rightarrow \boldsymbol{p} = \bar{\boldsymbol{p}}.$$

Interested readers are invited to consult the following references for practical examples of identifiability for analytical [7], ordinary differential [6], and partial differential models [15, 16].

Now, Definition 3.1 is applied to the ODE model (2.5) for the parameters $\boldsymbol{p} = (\alpha, C_{max}, g)$ that stand for $\boldsymbol{p}^0 = (\alpha^0, C_{max}^0, g^0)$ in (2.2) or $\boldsymbol{p}^{rad} = (\alpha^{rad}, C_{max}^{rad}, g^{rad})$ in (2.3), depending on the experimental dataset considered for the parameter estimation problem.

We assume two sets of observable C and $\bar{C}$ associated with the parameters $\boldsymbol{p}$ and $\bar{\boldsymbol{p}}$, respectively. Both functions verify the ODE equation (2.5). Thus, we have:

$$\frac{dC}{dt} = \alpha C \left(1 - \frac{C}{C_{max}} \right) - g C \tag{3.1}$$

and

$$\frac{d\bar{C}}{dt} = \bar{\alpha} \bar{C} \left(1 - \frac{\bar{C}}{\bar{C}_{max}} \right) - \bar{g} \bar{C}. \tag{3.2}$$

Now, we assume that $\forall t \in [0, T], C = \bar{C}$ and so $\forall t \in [0, T], \frac{dC}{dt} = \frac{d\bar{C}}{dt}$. Then, from Equations (3.1) and (3.2), we obtain:

$$\left((\alpha - g) - (\bar{\alpha} - \bar{g}) \right) C(t) - \left(\frac{\alpha}{C_{max}} - \frac{\bar{\alpha}}{\bar{C}_{max}} \right) C^2(t) = 0, \quad \forall t \in [0, T]. \tag{3.3}$$

Assuming that C is a non-constant and positive function in $[0, T]$, we immediately obtain that:

$$\begin{cases} (\alpha - g) = (\bar{\alpha} - \bar{g}), \\ \dfrac{\alpha}{C_{max}} = \dfrac{\bar{\alpha}}{\bar{C}_{max}}. \end{cases} \tag{3.4}$$

Equation (3.4) shows that Definition 3.1 is not satisfied for the ODE model (2.5) with the parameters $\boldsymbol{p} = (\alpha, C_{max}, g)$. But the combination of parameters $\left(\dfrac{\alpha}{C_{max}}, \alpha - g \right)$ is structurally identifiable in

the model. Therefore, Equation (2.5) is slightly changed and the following mathematical model, with parameters (a, b) that are structurally identifiable, is proposed for further investigations:

$$\begin{cases} \dfrac{dC}{dt} = a\,C^2 + b\,C, & t \in [0, T] \\ C(0) = C_0, \end{cases} \tag{3.5}$$

with parameters a and b defined by:

$$a = -\frac{\alpha}{C_{max}}\ (< 0)\,, \qquad b = \alpha - g\ (> 0). \tag{3.6}$$

In what follows, we will denote by $C_{a,b}$ the solution of Eq (3.5). Note that from identified parameters $a\,(day^{-1})$ and $b\,(day^{-1})$, the parameters (α, C_{max}, g) can be retrieved only if one of the three parameters is known *a priori*. In [19], authors defined the carrying capacity C_{max} as the M-times increase in the steady state value of a population of cancer cells, i.e. in which the system reaches equilibrium and the number of cancer cells remains constant over time:

$$C_{max} = M\,C_\infty\,, \tag{3.7}$$

with $M > 1$ a given coefficient and, according to (3.5),

$$C_\infty = \lim_{t \to +\infty} C_{a,b}(t) = -\frac{b}{a}. \tag{3.8}$$

In the end, given Eqs (3.7) and (3.6), parameters α and g are retrieved through parameters a and b using the following relations:

$$\begin{cases} \alpha = -a\,M\,C_\infty = M\,b, \\ g = b(M - 1). \end{cases} \tag{3.9}$$

Remark 1. *Eq (3.9) implies that the parameters α and g are related in the following form:*

$$\alpha = \frac{M}{M-1}g. \tag{3.10}$$

3.2. Practical identifiability analysis

This section investigates the practical identifiability of the unknown parameters a and b in the model (3.5). It analyses whether the observations are "rich" or sufficient to provide an accurate estimation of the unknowns. This concept is based on the parameters' sensitivity coefficients. For model (3.5), they are defined by:

$$\chi_a(t) = \frac{\partial C_{a,b}}{\partial a}\,, \qquad \chi_b(t) = \frac{\partial C_{a,b}}{\partial b}\,. \tag{3.11}$$

Several methods (finite-difference approximation, direct differentiation of the equation, complex step differentiation) are available to evaluate such quantities in Eq (3.11) (see [17] as a primary overview). However, in this work, an analytical solution holds for Eq (3.5):

$$C_{a,b}(t) = \frac{b\,C_0}{(a\,C_0 + b)\exp(-b\,t) - a\,C_0}\,. \tag{3.12}$$

Therefore, the parameters' sensitivity coefficients (3.11) are given analytically by:

$$\chi_a(t) = -\frac{b\,C_0\,(\,C_0\,\exp(-bt) - C_0\,)}{\big((\,a\,C_0 + b\,)\exp(-bt) - a\,C_0\big)^2}, \tag{3.13a}$$

$$\chi_b(t) = \frac{C_0}{(a\,C_0 + b)\exp(-bt) - \alpha\,C_0} - \frac{b\,C_0\big(\exp(-bt) - (\,a\,C_0 + b\,)\,t\,\exp(-bt)\big)}{\big((\,a\,C_0 + b\,)\exp(-bt) - \alpha\,C_0\big)^2}. \tag{3.13b}$$

With the sensitivity coefficients (3.13), one may investigate several issues for practical identifiability purposes [16]. First, if one sensitivity coefficient has low magnitude values with respect to the other and to the measurement noise, the model is poorly sensitive to the parameters. Next, if the sensitivity coefficients are linearly dependent, there is a correlation between the two parameters, and their simultaneous identification cannot be performed. Therefore, to get a reliable estimation of the parameters, it is necessary to have linearly independent sensitivity coefficients. The easiest way to check these issues is to plot one sensitivity coefficient according to the other for each time instant. This was shown in Figure 4. By analyzing such a plot, the sensitivity coefficient magnitude and correlation can be analyzed.

3.3. The parameter estimation problem statement

Consider the Eq (3.5), based on known data on the change in the number of cancer cells $C_{a,b}(t)$ over time, and it is necessary to identify the values of unknown parameters a and b. To solve this parameter estimation problem, an optimization problem was formulated, aiming to minimize the following objective function:

$$J(a,b) = \sum_{k=1}^{K}[C_{a,b}(t_k) - C_k]^2 \tag{3.14}$$

where the objective function $J(a,b)$ is the sum of least squared errors between the values of the function $C_{a,b}(t_k)$, solution of (3.5), and experimental data of C_k on a certain set of time points t_k, where K is the total number of experimental points over time.

To find optimal values of a and b, the objective function $J(a,b)$ is minimized:

$$(a^*, b^*) = \underset{(a,b)\in\mathcal{U}}{\arg\min} J(a,b), \tag{3.15}$$

with $\mathcal{U} = [-1, 0] \times [0, 1]$ being the set of acceptable parameters. The optimization problem can be solved using various methods, such as the gradient method [14], stochastic methods [1, 4, 8, 33], and others. In this work, we applied the Levenberg-Marquardt method [20, 21], a popular tool for solving a wide range of nonlinear optimization problems. The solution of the parameter estimation problem is implemented in MATLAB (version 8.6.0.267246 (R2015b)), using the *lsqcurvefit* function, with the Levenberg-Marquardt algorithm set in the *option*.

With this approach, the confidence interval (CI) of the retrieved parameter can be obtained. Thus, the uncertainty on the estimated parameter can be propagated in the model prediction by carrying out

derivative-based sensitivity analysis [29]. For this, a Taylor expansion of the first-order solution is written as:

$$C_{Tay}(t, a, b) = C_{a^*,b^*}(t) + \chi_{a^*}(t)(a - a^*) + \chi_{b^*}(t)(b - b^*) \tag{3.16}$$

where C_{a^*,b^*} is the solution of the ODE model (3.5), and χ_{a^*} and χ_{b^*} are the sensitivity coefficients from (3.13a) and (3.13b). Those quantities are evaluated using estimated parameters a^* and b^*. The terms $(a - a^*)$ and $(b - b^*)$ are set using the confidence intervals $[a_-^*, a_+^*]$ and $[b_-^*, b_+^*]$ of the retrieved parameters given by the optimization algorithm. More specifically, since in our case the sensitivity coefficients are positive for all time, those terms are defined using $a = a_+^*$ and $b = b_+^*$ for the upper bound confidence interval on the solution and $a = a_-^*$ and $b = b_-^*$ for the lower bound.

Equation (3.16) enables us to evaluate the influence of a small change of the estimated parameters (in their CI) on the predicted solution.

4. Parameter estimation results for ODE models

In this section, we consider the experimental data obtained from *in vivo* experiments on 31 mice with PCa bone metastasis, of which 19 were not treated, and 12 were treated (originally 13, however, 1 experiment had to be discarded because of operational issues). Data were acquired on days 0, 2, 5, 8, 12, and 15. Each data harvesting involved the use of luciferase as a standard indicator of tumor volume. Table 1 reports the mean volume at each investigation time point: **ctrl-data** refers to the control trend, while **rad-data** to treated cancer cells. Both **ctrl-data** and **rad-data** are used as C_k in Eq (3.14), depending on the problem being solved.

Table 1. The mean values of tumor cells from the *in vivo* data.

Day	C_k as **ctrl-data**	Standard deviation of **ctrl-data**	C_k as **rad-data**	Standard deviation of **rad-data**
0	24864	23994	13870	10771
2	112059	99399	41827	31738
5	577111	746142	70969	71813
8	1614381	1462355	122695	158071
12	2601221	1602812	255674	445121
15	4253605	2428198	419105	862375

4.1. The control data

The dataset of 19 control mice without treatment, their mean values C_k as **ctrl-data**, and standard deviation are illustrated in Figure 2.
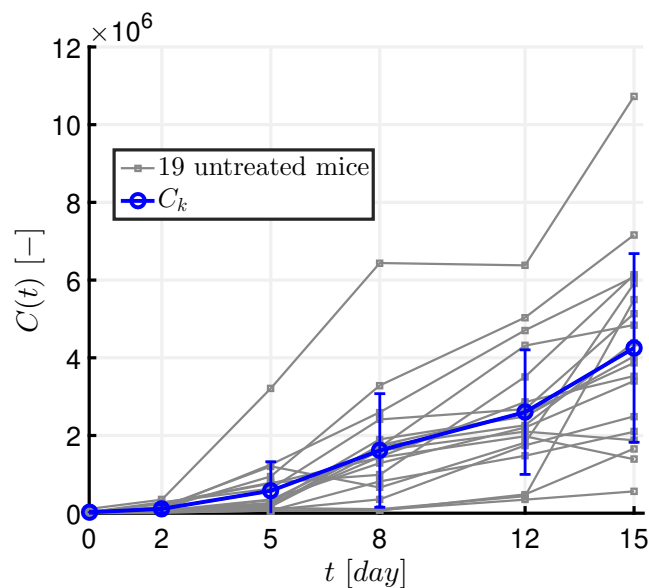
Figure 2. The dynamics of cancer cells in 19 untreated mice (gray lines), the mean value C_k as ***ctrl*-data** (marked blue line), and blue bars showing the standard deviation.
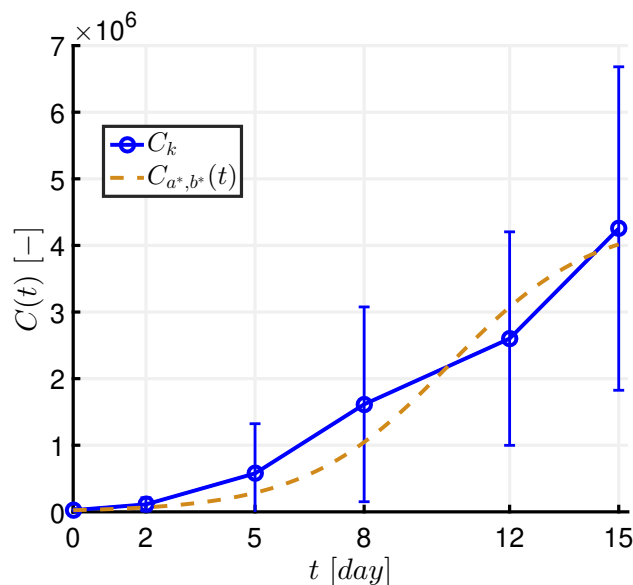

Figure 3. The graph of predicted dynamics of cancer cells' mean value with the estimated values of a^* and b^* parameters $C_{a^*,b^*}(t)$ is dashed brown line, while the blue marked line is the experimental data C_k as ***ctrl*-data** and the blue bars are the standard deviation.

The parameter estimation problem was calculated using data at 6 time points, distributed unevenly during the 15 days (see Table 1). Upper and lower limits of acceptable parameter values were set as $[-1, 0]$ and $[0, 1]$, respectively, to a and b. The initial guess for the parameters was chosen randomly, and the result did not change at all on each code compilation (more than 20 times). The numerical

results of solving the parameter estimation problem using ***ctrl*-data** as additional information are given in Table 2 and Figure 3.

Table 2. Identified parameters a^* and b^* of C_k as ***ctrl*-data**.

Parameter	Value	Upper CI	Lower CI	Units
a^*	$-1.13 \cdot 10^{-7}$	$-0.41 \cdot 10^{-7}$	$-1.84 \cdot 10^{-7}$	$[day^{-1}]$
b^*	0.50005	0.62	0.37	$[day^{-1}]$

Figure 3 presents the experimental data and the predicted number of cancer cells. The blue marked line shows the actual dynamics of changes in the number of cancer cells according to the experimental data C_k, and the brown dashed line represents the predicted dynamics of cancer cells' mean value $C_{a^*,b^*}(t)$ obtained by the estimated parameters a^* and b^*. Meanwhile, the blue bars accompanying the blue circles indicate the standard deviation of the data.
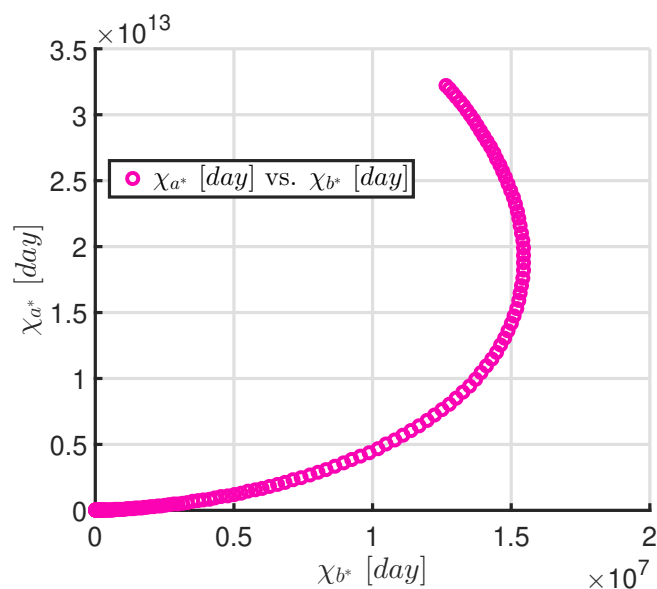

Figure 4. Dependency of the sensitivity functions.

The dependence of the sensitivity of the function $C_{a,b}$ for each time instant to the parameter a^* on the sensitivity to the parameter b^* is illustrated in Figure 4, where the graph shows an upward curve that increases slowly at first and then accelerates, indicating a nonlinear relationship between the parameters. Once a^* and b^* are estimated, the constant C_∞ can be calculated with $M = 2$ (see [19]). According to (3.8), we have:

$$C_{max}^0 = 2C_\infty = -2\frac{b^*}{a^*}. \tag{4.1}$$

Using (3.9), we obtain the following:

$$\begin{cases} \alpha^0 = 2b^*, \\ g^0 = b^*. \end{cases} \tag{4.2}$$

Table 3. Identified parameters $\boldsymbol{p}^0$ of ***ctrl*-data** C_k.

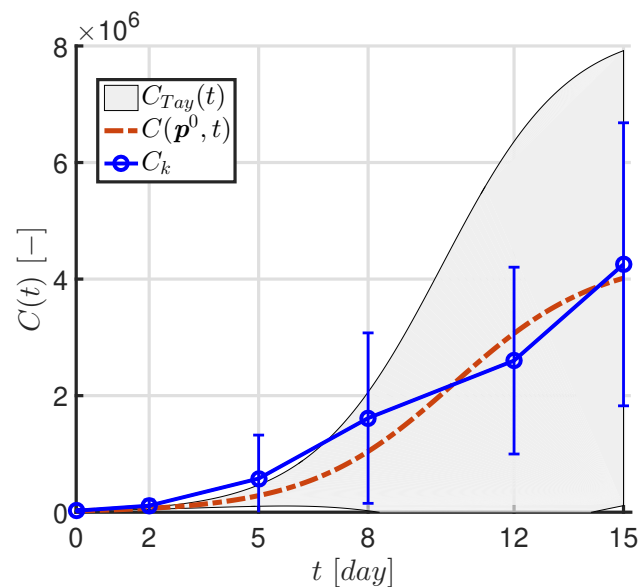| Parameter	Value	Units
α^0	1.0001	$[day^{-1}]$
C^0_{max}	8814147	$[-]$
g^0	0.50005	$[day^{-1}]$

Figure 5. Illustration of solution $C(\boldsymbol{p}^0, t)$ with estimated parameters $\boldsymbol{p}^0 = (\alpha^0, C^0_{max}, g^0)$ in comparison with experimental data C_k as ***ctrl*-data**, with indicated sensitivity region $C_{Tay}(t)$ and standard deviation bars.

Thus, the solution $C(\boldsymbol{p}^0, t)$, which depends on the obtained parameters $\boldsymbol{p}^0 = (\alpha^0, C^0_{max}, g^0)$ from Table 3, is represented in Figure 5 as a dash-dotted dark red line, whereas the blue line with markers is the experimental data ***ctrl*-data** C_k. The gray shaded area indicates the sensitivity region, reflecting the range of possible model values when varying the parameters in their confidence interval. The blue bars, representing the standard deviation, demonstrate the spread of the experimental data. The graph illustrates the correspondence of the analytical solution to the experimental data and shows the influence of the parameters on the model predictions. The magnitude of the model sensitivity is higher than the measurement standard deviation for $t = \{12, 15\}$ days. It indicates that the uncertainty on the retrieved parameters is too high to have a reliable model. Indeed, the predictions of the model tend to reach a threshold around $4 \cdot 10^6$, corresponding to the stationary state of the model, while the experimental data indicates a phase of growth. To improve the estimation, additional experimental data for $t > 15$ days are required.

4.2. The ^{223}Ra data

To study ^{223}Ra treatment applied to 12 mice, we used their mean values C_k as ***rad*-data** and standard deviation (Figure 6), considering 2 variants of mathematical models: with constant ^{223}Ra exposure (2.3) and taking into account ^{223}Ra decay over time (2.4).
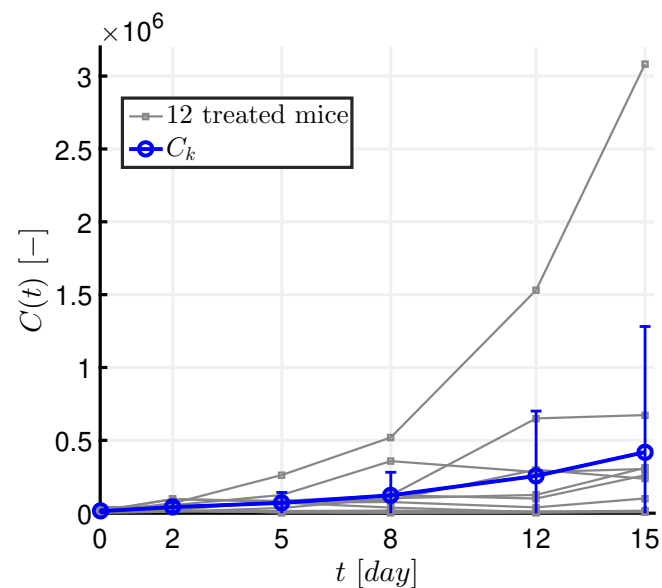
Figure 6. The dynamics of cancer cells in 12 treated mice (gray lines), the mean value C_k as ***rad*-data** of 12 data sets (blue marked line), and blue bars representing the standard deviation.

4.2.1. The ^{223}Ra data with constant mitosis and apoptosis rates

To solve the parameter estimation problem and identify the parameters $\mathbf{p}^{rad} = (\alpha^{rad}, C_{max}^{rad}, g^{rad})$, here the same protocol was used as for the control data (subsection 4.1). However in order to take into account the assumptions that $\alpha^{rad} < \alpha^0$ and $g^{rad} > g^0$ from (2.3) and Remark 1, the parameter C_{max}^{rad} was estimated with $M = 3$ in (3.7). Then the obtained values of the required parameters $\mathbf{p}^{rad} = (\alpha^{rad}, C_{max}^{rad}, g^{rad})$ are presented in Table 4.

Table 4. Identified parameters $\mathbf{p}^{rad}$ of ***rad*-data**.

Parameter	Value
α^{rad}	0.84677
C_{max}^{rad}	2178142
g^{rad}	0.56452

Figure 7 shows the dynamics of cancer cell growth under the influence of ^{223}Ra over time, where the blue line with markers represents the experimental data C_k as ***rad*-data**, and the green dash-dotted line is the solution $C(\boldsymbol{p}^{rad}, t)$ of the equation (2.5) taking into account the radiation effect, depending on the parameters $\boldsymbol{p}^{rad} = (\alpha^{rad}, C_{max}^{rad}, g^{rad})$. The gray area and blue bars are the model sensitivity area and measurement standard deviation, respectively. The solution $C(\boldsymbol{p}^{rad}, t)$ completely repeats the growth of the experimental data, which means that the estimated parameters are very satisfying. Furthermore, the magnitude of the model sensitivity is lower than the measurement standard deviation for all time. It indicates that the uncertainty on the retrieved parameters is small and that the model is reliable for this time interval.
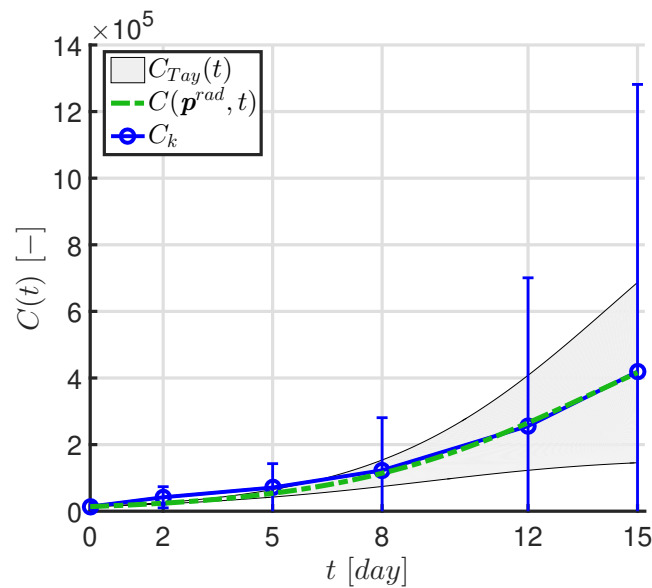
Figure 7. Illustration of solution $C(\boldsymbol{p}^{rad}, t)$ with estimated parameters $\boldsymbol{p}^{rad} = (\alpha^{rad}, C_{max}^{rad}, g^{rad})$ in comparison with experimental data C_k as **rad-data**, with indicated sensitivity region $C_{Tay}(t)$ and standard deviation bars.

4.2.2. The ^{223}Ra data with taking into account decay over time

Let us now consider an alternative and more accurate model that takes into account the decay of ^{223}Ra, namely equation (2.5) with diffusion, mitosis, and apoptosis parameters satisfying (2.4). There is no analytical solution for this model, so the solution of the direct problem was obtained in MATLAB using the *ODE45* function, which implements the explicit Runge-Kutta method of the 4th and 5th order with a variable step.

For Eq (2.4), the required values of α^0 and g^0 are shown in Table 3, the value of carrying capacity C_{max}^{rad} is shown in Table 4, and τ (day) was obtained from the following equation [23, 24]:

$$\tau = \frac{T_{1/2}}{\ln 2} = 15.89, \tag{4.3}$$

where $T_{1/2} = 11$ days, since it is the half-life time period of ^{223}Ra. We estimate the value of parameter r by minimizing an objective function similar to (3.14). Note that the obtained solution of this model is called $C(\boldsymbol{p}^r, t)$, with $\boldsymbol{p}^r = (r, C_{max}^{rad}, \tau)$.

Table 5. The values of the estimated parameter of treatment aggressiveness r.

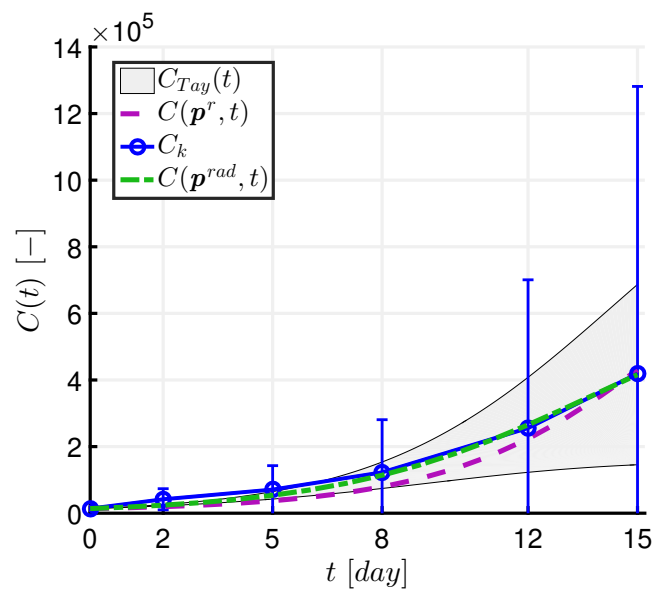| Parameter	Value	Upper CI	Lower CI	Units
r	0.23	0.21	0.25	$[-]$

Figure 8. The comparison of the growth of cancer cells over time for different models: with constant rates (green dash-dotted line) and with time dependence (purple dashed line).

Figure 8 illustrates a comparison of the growth of cancer cells over time for different models: with constant rates and with time-dependent rates. The blue marked line shows the experimental data C_k as **rad-data**, $C(\boldsymbol{p}^r, t)$ (the purple dashed line) corresponds to the model with time dependence of the decay of ^{223}Ra, and $C(\boldsymbol{p}^{rad}, t)$ (the green dash-dotted line) corresponds to the model without taking into account the decay over time. The gray area and blue bars are the model sensitivity area and measurement standard deviation, respectively.

Figure 9 shows changes in the values of mitosis and apoptotic rates for different scenarios: without treatment, with treatment employing constant coefficients, and with treatment considering time-dependence coefficients according to ^{223}Ra decay. The values of α^0 and g^0 remain constant throughout the observation period, as do the values of the parameters for the treatment with constant coefficients (α^{rad} and g^{rad}). Whereas the parameters $\alpha(t)$ and $g(t)$ show a dynamic change over time: $\alpha(t)$ tends to increase, and $g(t)$ to decrease. This reflects the time dependence of the treatment effect, where the treatment parameters change. The graph shows that at the initial time points, the effect of the therapy slows the mitosis rate $\alpha(t)$ of cancer cells (at a level of about 0.8, compared to 0.84 of α^{rad}) and increases the rate of their apoptosis $g(t)$ (approximately 0.66 versus 0.56 of g^{rad}), while by the end of the period, mitosis increases to a level at about 0.92 (compared to 1.0001 of α^0 without treatment), and apoptosis falls to a level of about 0.54, slightly lower than the value of g^{rad}.

To prove the usage of the time-dependent trend of ^{223}Ra and its activity in our mathematical model, the simulation was done until the 50th day and the results of the estimation (Figure 10) replicated the *in vivo* and *in silico* tests of [10], reaching nearly 0% effectiveness by days $45-50$ ($g(t = 50)$ is very close to g^0). Furthermore, as can be seen from the graph, the effect of the ^{223}Ra application decreased by 50% by day 11, which corresponds to its half-life time [10, 12].
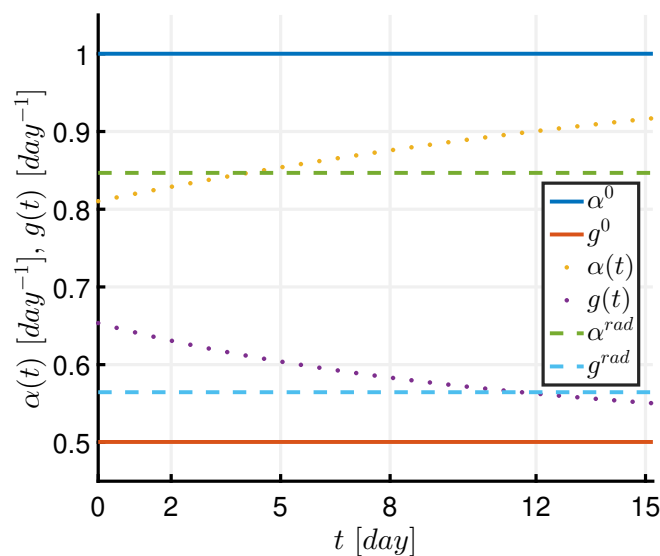
Figure 9. The changes in the values of mitosis and apoptotic rates for different scenarios: without treatment (continuous lines, designated as α^0 and g^0), with treatment with constant coefficients (dashed lines, designated as α^{rad} and g^{rad}), and with treatment with time-dependent coefficients (dotted lines $\alpha(t)$ and $g(t)$).
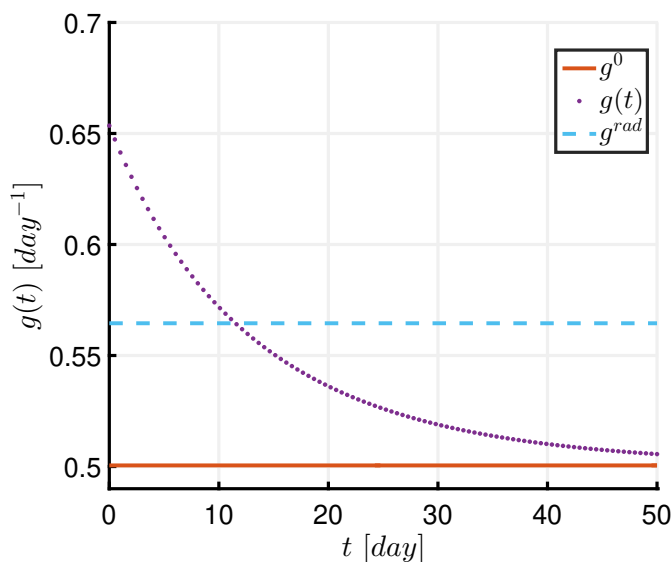

Figure 10. The changes in the values of apoptosis rates for different scenarios: g^0 (without treatment, represented by the dark orange solid line), g^{rad} (with treatment with constant coefficients, represented by the blue dashed line), and $g(t)$ (with treatment with time-dependent coefficients, represented by the purple dotted line).

5. Tumor growth simulations with the PDE model

In section 4, the parameters $p = (\alpha(t), C_{max}, g(t))$ in (2.1) have been identified, under the assumption that the diffusion coefficient ρ is small, for 3 cases: without treatment p^0 (see Table 3), with constant treatment p^{rad} (see Table 4), and with time-dependent treatment p^r (see (4.3) and Table 5). These results establish a basis to solve the partial differential equation (2.1).

Numerical modeling of the PDE problem was performed in Python (version 3.10.12) using the FEniCS package (2019.2.0.13.dev0) [2], which uses the finite element method (FEM) [9, 34]. The calculation was performed in a square region $\Omega = [-1, 1]cm \times [-1, 1]cm$, and the mesh was obtained by dividing Ω into $2 \cdot 10^4$ triangular elements.
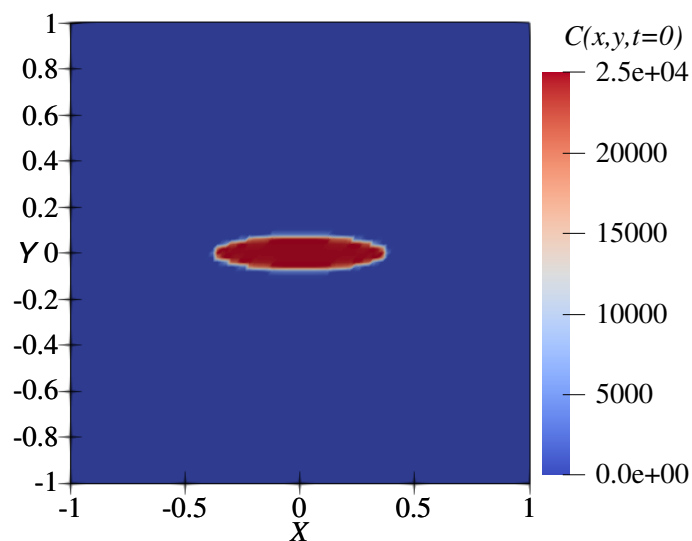
Figure 11. Color map of the density (number) of the cancer-cell distribution in the bone-cancer interaction region at $t = 0$. The blue area represents bone, while the ellipsoidal red area represents cancer. The scale on the right displays the numerical density values, ranging from 0 to 25000.

We discretized Eq (2.1) in space with a P_2-finite element method, and in time with an implicit Euler scheme. The time step was chosen to be fixed and equal to $\Delta t = 0.1$ (day). We chose the carrying capacity $\hat{C}_{max} = 10^6$ and the diffusion coefficients $\rho^0 = \rho^{rad} = 10^{-4} \, cm^2/day^{-1}$. The tumor geometry was initially described as an ellipse (see Table 6), and the initial total number of cancer cells was taken equal to the initial number of cancer cells of **ctrl-data**, evenly distributed on the area of the ellipse.

The density (number) of the cancer-cell distribution in the region of interest at time $t = 0$ is shown in Figure 11. The blue area corresponds to bone tissue. In the center of the image, an ellipsoidal area is highlighted, colored in red tones, which corresponds to the cancer tumor zone.

Figures 12−14 illustrate the simulation results at time $t = 15 \, day$ in the case of no treatment (Figure 12), meaning the use of parameters p^0, with constant treatment (Figure 13) using parameters p^{rad}, and time-dependent ^{223}Ra treatment (Figure 14) using parameters p^r. To illustrate the difference in the simulation results of all 3 cases, the numerical density values were rescaled from the range 0-25000 to the range 0-350000.
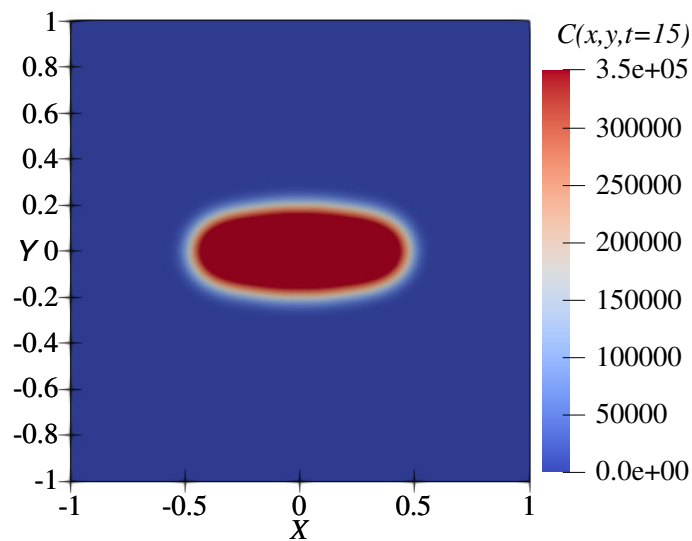
Figure 12. Color map of the density (number) of the cancer-cell distribution in the bone-cancer interaction region at $t = 15$ *day* without treatment (p^0). The blue area represents bone with low density values, while the ellipsoidal red area represents cancer with increased density. The scale on the right displays the numerical density values, ranging from 0 to 350000.
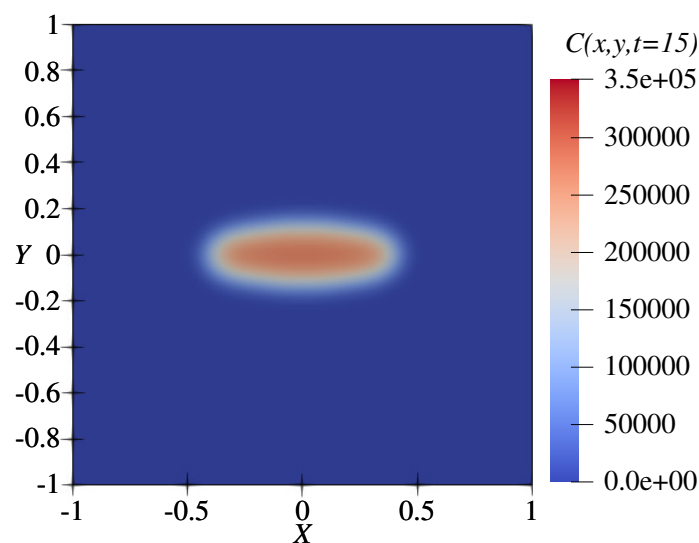

Figure 13. Color map of the density (number) of the cancer-cell distribution in the bone-cancer interaction region at $t = 15$ *day* with constant treatment (p^{rad}).

As can be seen, the greatest tumor growth was demonstrated in Figure 12, where there was no treatment. The clearly defined density of the ellipsoid area exceeding 300000 units indicates disease progression, and the bright contrast between cancer cells and bone tissue indicates the absence of regression. The continuous ^{223}Ra treatment (Figure 13) shows a significant impact on the invasion and growth of the tumor, due to less defined contours and a decline in the intensity of the red area. The

treatment has a visible effect on the tumor, slowing down further growth.

The most pronounced treatment effectiveness compared to the previous ones is demonstrated in Figure 14 by the time-dependent treatment scenario, as indicated by the small tumor size, very blurred boundaries, and a weak area with low density, with maximum values less than 150000 units.
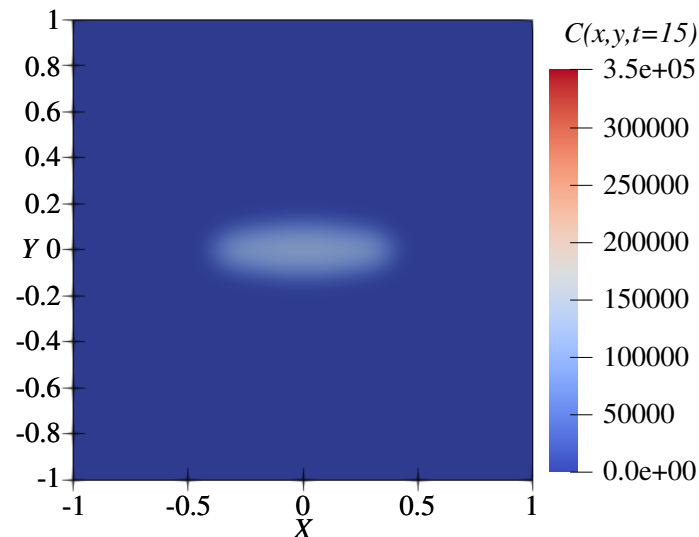

Figure 14. Color map of the density (number) of the cancer-cell distribution in the bone-cancer interaction region at $t = 15$ *day* with time-dependent ^{223}Ra treatment ($\boldsymbol{p^r}$).

Table 6 presents the radii of the ellipsoidal regions representing the tumor in the three scenarios, at time $t = 15$ *day*. The comparison shows that no treatment ($\boldsymbol{p^0}$) results in a large tumor invasion, while constant ^{223}Ra treatment ($\boldsymbol{p^{rad}}$) and time-dependent ^{223}Ra treatment ($\boldsymbol{p^r}$) have a significant positive effect, reducing the tumor growth.

Table 6. Comparison of radii values at $t = 0$ and $t = 15$ days on 3 scenarios.

Radius	$t = 0$	$t = 15$	$t = 15$	$t = 15$	Direction	Units
		$\boldsymbol{p^0}$	$\boldsymbol{p^{rad}}$	$\boldsymbol{p^r}$		
r_1	0.375	0.553	0.489	0.438	x-axis	[*cm*]
r_2	0.075	0.273	0.213	0.169	y-axis	[*cm*]

6. Conclusions

We developed a versatile PDE model to investigate the effects of ^{223}Ra therapy on PCa bone metastasis. Mitosis and apoptosis coefficients of the model have been calibrated using data from 31 mice with metastatic lesions, both treated and untreated. While available ABMs offer biologically precise results, they are limited to small scales, such as individual tumors. In contrast, our PDE model operates on a larger scale encompassing the entire affected organ while also significantly reducing computational costs. Importantly, our model accurately reflects experimental realities, making it a more efficient and scalable alternative to existing ABM approaches in studying bone metastasis

response to ^{223}Ra. Future work will address the model's consideration of the distance from bone in ^{223}Ra efficacy.

Author contributions

Zholaman Bektemessov: Formal analysis, investigation, visualization, writing – original draft; Laurence Cherfils, Stefano Casarin: Conceptualization; Laurence Cherfils, Cyrille Allery, Julien Berger: Supervision; Elisa Serafini, Eleonora Dondossola, Stefano Casarin: Data curation. ZB, LC, CA, JB, ES, ED, SC: Writing – review and editing. All authors contributed to the article and approved the submitted version.

Acknowledgments

Conflict of interest

The authors declare that there is no conflict of interest in this paper.

References

1. E. Aarts, J. Korst, *Simulated annealing and Boltzmann machines: A stochastic approach to combinatorial optimization and neural computing*, John Wiley, 1989. https://doi.org/10.2307/2008816

2. M. S. Alnæs, J. Blechta, J. Hake, A. Johansson, B. Kehlet, A. Logg, et al., The FEniCS Project Version 1.5, *Archive of Numerical Software,* **3** (2015), 9–23. https://doi.org/10.11588/ans.2015.100.20553

3. C. Baldessari, S. Pipitone, E. Molinaro, K. Cerma, M. Fanelli, C. Nasso, et al., Bone metastases and health in prostate cancer: From pathophysiology to clinical implications, *Cancers (Basel),* **15** (2023), 1–24. https://doi.org/10.3390/cancers15051518

4. G. Beni, From Swarm Intelligence to Swarm Robotics, *Lecture Notes in Computer Science,* **3342** (2005), 1–9. https://doi.org/10.1007/978-3-540-30552-1_1

5. O. Bergengren, K. R. Pekala, K. Matsoukas, J. Fainberg, S. F. Mungovan, O. Bratt, et al., 2022 update on prostate cancer epidemiology and risk factors—a systematic review, *European Urology,* **84** (2023), 191–206. https://doi.org/10.1016/j.eururo.2023.04.021

6. J. Berger, D. Dutykh, Evaluation of the reliability of building energy performance models for parameter estimation, *Journal Computational Technologies,* **24** (2019), 4–32. https://doi.org/10.25743/ICT.2019.24.3.002

7. J. Berger, T. Colinart, B. R. Loiola, H. R. B. Orlande, Parameter estimation and model selection for water sorption in a wood fibre material, *Wood Science and Technology,* **6** (2020), 1423–1446. https://doi.org/10.1007/s00226-020-01206-0

8. D. Bertsimas, J. Tsitsiklis, Simulated Annealing, *Statistical Science,* **8** (1993), 10–15. https://doi.org/10.1214/ss/1177011077

9. S. C. Brenner, L. R. Scott, *The Mathematical Theory of Finite Element Methods*, Springer, 2007. https://doi.org/10.1007/978-0-387-75934-0

10. S. Casarin, E. Dondossola, An agent-based model of prostate Cancer bone metastasis progression and response to Radium223, *BMC Cancer,* **20** (2020), 1–19. https://doi.org/10.1186/s12885-020-07084-w

11. P. Colli, H. Gomez, G. Lorenzo, G. Marinoschi, A. Reali, E. Rocca, Mathematical analysis and simulation study of a phase-field model of prostate cancer growth with chemotherapy and antiangiogenic therapy effects, *Math. Models Methods Appl. Sci.,* **30** (2020), 1253–1295. https://doi.org/10.1142/S0218202520500220

12. E. Deshayes, M. Roumiguie, C. Thibault, P. Beuzeboc, F. Cachin, C. Hennequin, et al., Radium 223 dichloride for prostate cancer treatment, *Drug design, development and therapy,* **11** (2017), 2643–2651. https://doi.org/10.2147/DDDT.S122417

13. E. Dondossola, S. Casarin, C. Paindelli, E. M. De-Juan-Pardo, D. W. Hutmacher, C. J. Logothetis, et al., Radium 223-Mediated Zonal cytotoxicity of Prostate Cancer in Bone, *JNCI: Journal of the National Cancer Institute,* **111** (2019), 1042–1050. https://doi.org/10.1093/jnci/djz007

14. C. B. Haskell, The method of steepest descent for non-linear minimization problems, *Quarterly of Applied Mathematics,* **2** (1944), 258–261. http://www.jstor.org/stable/43633461

15. A. Jumabekova, J. Berger, D. Dutykh, H. Le Meur, A. Foucquier, M. Pailha, et al., An efficient numerical model for liquid water uptake in porous material and its parameter estimation, *Numerical Heat Transfer, Part A: Applications,* **75** (2019), 110–136. https://doi.org/10.1080/10407782.2018.1562739

16. A. Jumabekova, J. Berger, A. Foucquier, G. S. Dulikravich, Searching an optimal experiment observation sequence to estimate the thermal properties of a multilayer wall under real climate conditions, *International Journal of Heat and Mass Transfer,* **155** (2020), 1–28. https://doi.org/10.1016/j.ijheatmasstransfer.2020.119810

17. A. Jumabekova, J. Berger, A. Foucquier, An efficient sensitivity analysis for energy performance of building envelope: A continuous derivative based approach, *Building Simulation,* **14** (2021), 909–930. https://doi.org/10.1007/s12273-020-0712-4

18. S. Kabanikhin, M. Bektemesov, O. Krivorotko, Z. Bektemessov, Practical identifiability of mathematical models of biomedical processes, *Journal of Physics: Conference Series,* **2092** (2021), 1–12. https://doi.org/10.1088/1742-6596/2092/1/012014

19. T. Le, S. Su, A. Kirshtein, L. Shahriyari, Data-Driven Mathematical Model of Osteosarcoma, *Cancers (Basel),* **13** (2021), 1–34. https://doi.org/10.3390/cancers13102367

20. K. Levenberg, A Method for the Solution of Certain Non-Linear Problems in Least Squares, *Quarterly of Applied Mathematics,* **2** (1944), 164–168. https://doi.org/10.1090/qam/10666

21. D. Marquardt, An Algorithm for Least-Squares Estimation of Nonlinear Parameters, *SIAM Journal on Applied Mathematics,* **11** (1963), 431–441. https://doi.org/10.1137/0111030

22. P. Mukherjee, S. Roy, D. Ghosh, S. K. Nandi, Role of animal models in biomedical research: a review, *Lab. Anim. Res.,* **38** (2022), 1–17. https://doi.org/10.1186/s42826-022-00128-1

23. R. A. Muller, *Physics and Technology for Future Presidents: An Introduction to the Essential Physics Every World Leader Needs to Know*, Princeton, New Jercey: Princeton University Press, 2010.

24. C. R. Nave. *"Radioactive Half-Life". HyperPhysics. Georgia State University*, "Radioactive Half-Life". HyperPhysics. Georgia State University, 2024. Available from: `http://hyperphysics.phy-astr.gsu.edu/hbase/hframe.html`.

25. C. Paindelli, S. Casarin, F. Wang, L. Diaz-Gomez, J. Zhang, A. G. Mikos, et al., Enhancing ^{223}Ra Tretment Efficacy by Anti-β1 Integrin Targeting, *J. Nucl. Med.,* **63** (2022), 1039–1045. https://doi.org/10.2967/jnumed.121.262743

26. C. Parker, S. Nilsson, D. Heinrich, S. I. Helle, J. M. O'Sullivan, S. D. Fosså, et al., Alpha emitter radium-223 and survival in metastatic prostate cancer, *N. Engl. J. Med.,* **369** (2013), 213–223. https://doi.org/10.1056/NEJMoa1213755

27. H. Raad, C. Allery, L. Cherfils, C. Guillevin, A. Miranville, T. Sookiew, et al., Simulation of tumor density evolution upon chemotherapy alone or combined with a treatment to reduce lactate levels, *AIMS Mathematics,* **9** (2024), 5250–5268. https://doi.org/10.3934/math.2024254

28. T. Roubièek, *Nonlinear Partial Differential Equations with Applications*, 2 Eds., Birkhauser, 2013. https://doi.org/10.1007/978-3-0348-0513-1

29. I. M. Sobol, S. Kucherenko, Derivative based global sensitivity measures and their link with global sensitivity indices, *Mathematics and Computers in Simulation,* **79** (2009), 3009–3017. https://doi.org/10.1016/j.matcom.2009.01.023

30. P. Tracqui, G. C. Cruywagen, D. E. Woodward, G. T. Bartoo, J. D. Murray, E. C. Alvord, A mathematical model of glioma growth: the effect of chemotherapy on spatio-temporal growth, *Cell Proliferation,* **28** (1995), 17–31. https://doi.org/10.1111/j.1365-2184.1995.tb00036.x

31. E. Walter, Y. Lecourtier, Global approaches to identifiability testing for linear and nonlinear state space models, *Mathematics and Computers in Simulation,* **24** (1982), 472–482. https://doi.org/10.1016/0378-4754(82)90645-0

32. F. Wu, Y. Zhou, L. Li, X. Shen, G. Chen, X. Wang, et al., Computational approaches in preclinical studies on drug discovery and development, *Front Chem.,* **8** (2020), 1–32. https://doi.org/10.3389/fchem.2020.00726

33. X. S. Yang, *Nature-Inspired Optimization Algorithms*, Elsevier, 2014. https://doi.org/10.1016/C2013-0-01368-0

34. O. C. Zienkiewicz, R. L. Taylor, *The Finite Element Method*, Volume 1: The Basis, Butterworth-Heinemann, 2000.